Multi-chain slip-spring simulations for branch polymers

*Yuichi Masubuchi

Department of Materials Physics, Nagoya University, Japan.

*Correspondence:

e-mail mas@mp.pse.nagoya-u.ac.jp

Tel +81-51-7892551

Submitted to Macromolecules, 2018, Aug. 12

Revised version, 2018, Oct. 16

2nd Revision, 2018, Nov. 22

Published (Web), 2018, Dec. 4

ABSTRACT

Although the tube models have attained remarkable success, development of simulation method for entangled branch polymer dynamics is still a challenge. In this study, the multi-chain slip-spring model has been examined to branch polymers for the first time. In the model, the bead-spring chains are dispersed in the simulation box, and the entanglement is mimicked by the virtual spring so-called slip-spring, which connects the chains and hops along the chain. The slip-springs are created and destructed only at the chain ends. Besides, for the relaxation of entanglements formed between the backbone chains in the branch polymers, the hopping of slip-spring across the branch point (SHAB) is additionally allowed when the branching arm relaxes. The simulation results for symmetric and asymmetric star and H branch polymers are in semi-quantitative agreement with experimental and earlier simulation data extracted from the literature. Although the proposed simulation is compatible with the data for scarcely entangled systems, due to the computational difficulties the test against well-entangled systems was remained unperformed, and the details of SHAB implementation remains open.

KEYWORDS

Viscoelasticity, diffusion, coarse-graining, entanglement, branch point motion

INTRODUCTION

Lots of attempts have been made to describe the dynamics of branch polymers in the entangled state[1]. The theoretical development has been made owing to the tube picture, in which the entanglement effects for a test molecule by the surrounding molecules are cast into a tube-shaped constraint[2,3]. Since the branching point prevents the sliding of the molecule along the tube, the dominating relaxation mode is the retraction of the branching arm towards the branch point. Initiated by the pioneering work by Doi and Kuzuu[4], molecular theories have been developed for quantitative description of linear viscoelasticity of star polymers for which the molecular weights of branching arms are identical[5–7]. Meanwhile, further development has been elaborated for the other classes of branch polymers, for which the sliding motion of backbone activated after the retraction of branching arms is the dominating relaxation mechanism. McLeish[8] introduced such a hierarchical relaxation idea, and applicability of the modified theory has been confirmed for H[9], comb[10,11] and asymmetric star polymers[12]. The hierarchical relaxation idea has been followed by the code developments for further complicated branching structures[13–17]. The theory for non-linear viscoelasticity has been developed as well by implementing the branch point withdrawal activated under fast flows[18,19].

Apart from the theories mentioned above, molecular dynamics simulation is a straightforward option. Indeed, the tube modeling is difficult for some problems with structural and dynamical inhomogeneity. For entangled branch polymers, despite the technical difficulties including equilibration[20–22], several attempts have been performed for prediction of long-time behaviors[23–26]. The other smart direction is tests of the assumptions in molecular theories, such as the branch point dynamics assumed in the hierarchical picture[27–29]. Studying the effects of branching on the structure of the entanglement network[30] is another interesting direction as well. In most of the attempts mentioned above, the coarse-grained bead-spring model[31] is used. However, the computational efficiency is not practically sufficient to reproduce characteristic features of entangled branch polymers. For example, quantitative comparison to experimental data for viscoelastic spectrum has never been reported to our knowledge.

Further coarse-graining has been attempted than bead-spring models to trace the long-time dynamics of branch polymers. Padding and Briels[32] have developed a smart algorithm so-called TWENTANGLEMENT, in which the chain crossing is prohibited according to the geometry. Kumar and Larson[33] have proposed the inter-bonds interaction

so-called segment repulsive potential. Although these techniques have been applied to star polymers[34,35], the benefit in the reduction of computational costs seems not sufficient. Kindt and Briels[36] have proposed a further coarse-grained description so-called RaPiD, in which a single particle represents each polymer molecule, and the effects of entanglement are embedded into the inter-particle interactions. This approach is quite useful on the computational efficiency, and it has been tested for a star polymer system[37]. However, design of the inter-particle interaction is not straightforward. The multi-chain slip-link simulation[38] is an approach located in the niche between the technique disallowing chain crossing and the inter-particle modeling of entanglements. In this modeling, the entanglements among polymers are replaced by slip-links that bundle two polymer chains in a pair. Due to the neglected degrees of freedom between entanglements, this model attains a considerable reduction in computational costs, yet it naturally implements some multi-chain effects such as thermal and convective constraint release. This model has reproduced a variety of rheological phenomena for branch polymers semi-quantitatively for linear and non-linear viscoelasticity of star[39,40], H[15,41], pompom[42] and comb[43] polymers. However, the problem of this modeling is that the molecular motion is calculated concerning the dynamics of entanglement, and thus, extensions towards further complex systems with specific inter-molecular interactions are fundamentally

challenging due to the lack of the requisite degree of freedom.

A promising approach is the multi-chain slip-spring model[44–47] that considers the dynamics of a lot of Rouse chains dispersed in the simulation box. As a natural extension of the single chain version[48], in this approach the entanglement effect is replaced by virtual springs that connects two Rouse beads in a pair. The springs slide along the chain, and they are created and removed at chain ends. Depending on the density of virtual springs, each Rouse bead carries a specific molecular weight corresponding to several beads for the conventional bead-spring simulations. This reduction of the degrees of freedom attains less computations. The lack of hard-core interactions helps the calculation as well. Consequently, entangled polymer dynamics can be traced with much less computational costs than the bead-spring simulations. Meanwhile, inter-molecular interactions can be reasonably implemented for the Rouse beads. For instance, the attempts have been made for block copolymers[46] and polymer solutions[49]. The systematic coarse-graining has also been attempted from the atomistic molecular simulations[50,51].

In this study, the multi-chain slip-spring model is extended to branch polymers. The extension is straightforward except the topological change around the branch point. As

discussed in the tube model[8] and the slip-link model[15], the branch point hinders the topological dynamics of entanglement. The simple idea is disallowing penetration of entanglement across the branch point to conserve the topology around branch point. The earlier models for star polymers[4–7] are constructed on the basis of this conserved topology, in which the chain sliding is not allowed at the branch point. This idea works well for star polymers for which the molecular weights of branching arms are identical to each other. However, further consideration is necessary for the other classes of branch polymers for which the sliding motion of the backbone chain is the dominant relaxation mechanism. In particular, polymers with multiple branch points per molecule never relax under the conserved topology. In the present study, in accordance with the earlier tube[8] and slip-link[15,17] models, the topological change between entanglement and branch point is triggered by the relaxation of the branching arm. Namely, a slip-spring is allowed to hop across the adjacent branch point if the branching arm does not carry any slip-spring at that moment. The results are compared with the literature data for the bead-spring simulations and the experiments for star and H branch polymers. The comparison is made to the results for multi-chain slip-link simulations as well.

MODEL AND SIMULATIONS

The multi-chain slip-spring (MCSS) model proposed by Uneyama and Masubuchi[44] was extended. In the model, polymers are replaced by Rouse chains consisting of beads and springs. The chains are dispersed in a simulation box with a specific beads density and connected with each other via virtual springs that mimic entanglements. Because the virtual springs hop between consecutive beads along the chain, they are called slip-springs. The state variables are the bead position and the connectivity of slip-springs. The total free energy of the system is given by

$$\frac{F}{kT} = \frac{3}{2b^2}\sum_{i,k}\left(\mathbf{R}_{i,k+1} - \mathbf{R}_{i,k}\right)^2 + \frac{3}{2N_s b^2}\sum_{\alpha}\left(\mathbf{R}_{S_{\alpha,1},S_{\alpha,2}} - \mathbf{R}_{S_{\alpha,3},S_{\alpha,4}}\right)^2 + e^{\nu/kT}\sum_{i,k,j,l}\exp\left[-\frac{3}{2N_s b^2}\left(\mathbf{R}_{i,k} - \mathbf{R}_{j,l}\right)^2\right] \quad (1)$$

The first term of the right-hand side of eq 1 is the contribution of the Rouse springs, for which $\mathbf{R}_{i,k}$ is the position of beads, the indices stand for chain i and bead k. b is the bond length. The second term is the contribution of slip-springs. α is the index for the slip-spring, and S_α=$(S_{\alpha,1}, S_{\alpha,2}, S_{\alpha,3}, S_{\alpha,4})$ is the state of the spring α, for which the ends are connected at the bead $S_{\alpha,2}$ of chain $S_{\alpha,1}$ and the bead $S_{\alpha,4}$ of chain $S_{\alpha,3}$. N_s is the elastic parameter of the slip-springs. Because the second term plays a role of the attractive interaction between the beads on average, it disturbs the statistics of the Rouse chains. Since any effect of entanglement on chain statistics is not observed experimentally, the third term is thus added to the free energy to correctly eliminate the artifact of the

second term on the chain statistics. $e^{\nu/kT}$ is the activity of slip-springs[52], for which the grand canonical ensemble is assumed. Although the 3rd term has the form of a soft repulsive interaction potential, as mentioned above, the role of this term is to correct the chain statistics, and thus, no effect on the density fluctuations. Consequently, the compressibility of the present model is the same with that of an ideal gas, and different from the real polymer melts. Some recent studies have proposed systematic methods for the modeling of compressibility, yet utilized the slip-springs to mimic the entanglement effect[50,51].

From eq 1, the kinetic equations for the state variables can be derived according to the standard procedures. Namely, the equation of motion of the beads is the Langevin equation. For the slip-springs, the sliding kinetics along the chain and the creation and destruction events at chain ends are managed concerning the Glauber dynamics. See the earlier publication[44] for further details.

For the model extension to branch polymers, the sliding rule for slip-springs around branch point must be considered. In this study, from the hierarchical relaxation idea[8], the hopping of slip-springs across the branch point is allowed when the branching arm is

relaxed. Assume that there exists a slip-spring (red spring) connected to a bead next to a branch point as shown in Fig 1, and the anchoring points of the slip-spring attempts to hop over the branch point (red bead in Fig 1). The slip-spring hopping across the branch point is referred to as SHAB, hereafter. SHAB is allowed when the branching arm (yellow beads) does not carry any slip-spring at this moment. This criterion for the arm retraction can be modified. A possible alternative is according to the birth time of slip-springs, as proposed for the slip-link model earlier[53], though such an idea was not examined in this study.

In addition to the arm relaxation mentioned above, the acceptance of SHAB is managed by the Glauber dynamics as made for the usual sliding. In this respect, the acceptance ratio of SHAB may be different from the usual sliding because of the difference of the hopping distance along the chain, which is one bond for the usual sliding whereas it is two bonds for SHAB. If there exist multi-arms (q arms) from the branch point, SHAB is allowed only when $q-2$ arms relax at the same time. Then the anchoring point hops along the unrelaxed arms. As long as the conditions above are fulfilled, SHAB can reversibly, and the anchoring point of the slip-spring may hop back and forth across the branch point.

The branching arm without slip-spring corresponds to the full retraction state in the terminology of tube model, as proposed by Shanbhag and Larson[17] for the slip-link model. The correspondence to the arm retraction may suggest that the occurrence of SHAB is related to the chain conformation, although such a bias is not explicitly considered in the scheme proposed here. Concerning this issue, Ramírez-Hernández et al. [54] reported that there is not a significant correlation between the slip-spring number and the chain conformation for block copolymers under microscopic phase separation.

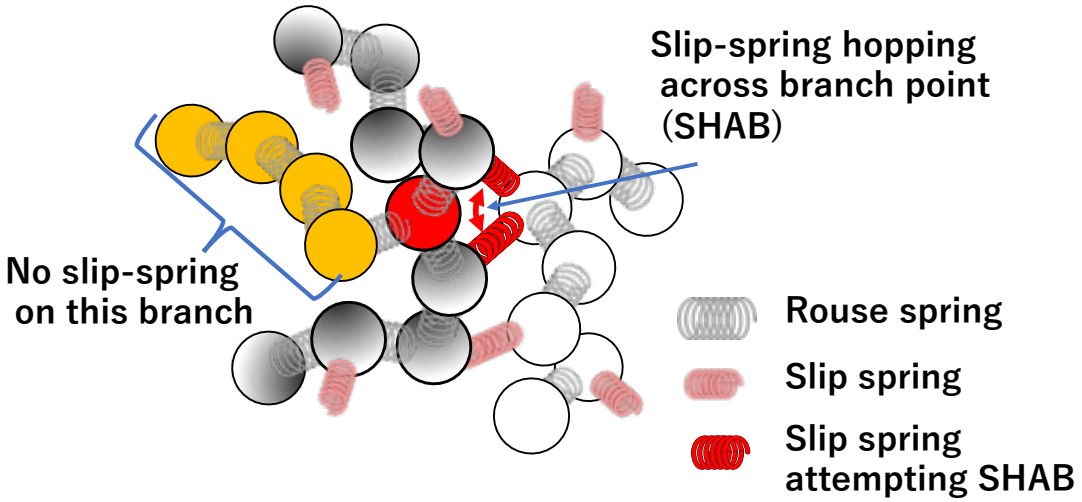

Figure 1 Schematic representation of the slip-spring hopping across the branch point (SHAB). Red, yellow, black and white beads are the branch point, the examined branch, the backbone, and the other chain, respectively. SHAB is activated when no slip-spring exists on the branching arm.

For comparison purpose, multi-chain slip-link simulations were also performed. Since the model used is the primitive chain network model[38], the simulation is referred to as PCN simulation hereafter. In the model, the entangled polymers are replaced by networks consisting of nodes, strands, and dangling ends. A path connecting dangling ends represent each polymer. At the network nodes, slip-links are placed to bundle two polymer chains in a pair to restrict the polymer motion perpendicular to the backbone. The dynamics of the system is described by the Brownian motion of the slip-links, the sliding motion of the chains through the slip-links, and the creation/destruction of the slip-links at the chain ends. For the branch polymers, a similar relaxation mechanism to SHAB has been introduced to permit the sliding motion of the chain at the branch points when the branching arm relaxes. Refer to the earlier publications[15,42] for further details of SHAB implemented in PCN.

The simulations were performed for linear, star-branch and H-branch polymers with various segment numbers per molecule. Periodic boundary condition was used with simulation box that is sufficiently larger than the dimension of molecules. The quiescent simulations were performed for large simulation time steps that are more than ten times

larger than the longest relaxation time of each system. For statistics, the data obtained from eight independent simulation runs were acquired for each case. The parameters for the simulations were the same as the previous study[55]. For the MCSS simulations, the bead density was 4, the virtual spring intensity N_s was 0.5, and the slip-spring activity $e^{\nu/kT}$ was 0.036. These parameters give the average segment number between two anchoring points of virtual springs along the chain as $N_e^{SS} = 3.5$. The cut-off length for the calculation of the 3rd term in the right-hand side of eq 1 was 3.2, with which the Gaussian chain statistics are reasonably maintained given that the sampling distance for the creation of new slip-spring is consistent[44]. For the PCN simulations, the segment number density was 10, and the osmotic parameter was 1.0. Figure 2 shows a snapshot of the MCSS simulation for the H polymer, for which the arms and the backbone consist of 17 beads.

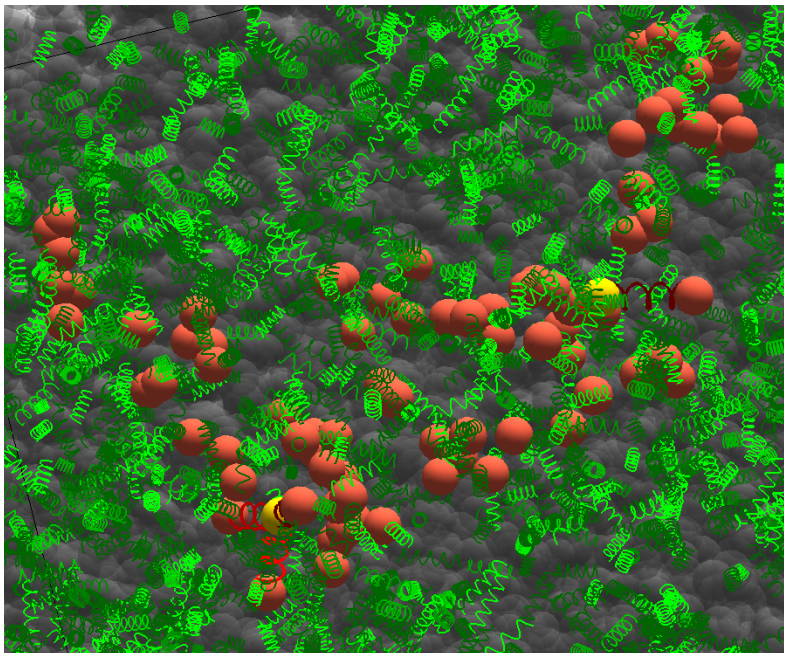

Figure 2 Snapshot of H polymer with 17 beads on the subchains for the arms and the backbone. Yellow beads are the branch points. Green springs are the dispersed slip-springs. Gray beads are the surrounding molecules.

The simulation results were converted by the scale-conversion factors that have been obtained for linear polymers. Among MCSS, PCN, and the standard bead-spring simulation proposed by Kremer and Grest (KG), the conversion relationships obtained for the segment number, length, time and modulus are as follows[55].

$$40N_{\mathrm{PCN}} = 8N_{\mathrm{MCSS}} = N_{\mathrm{KG}} \qquad (2)$$

$$6.2a_{\mathrm{PCN}} = 3.1b_{\mathrm{MCSS}} = \sigma_{\mathrm{KG}} \qquad (3)$$

$$1.3 \times 10^4\tau_{\mathrm{PCN}} = 750 \times 10^2\tau_{\mathrm{MCSS}} = \tau_{\mathrm{KG}} \qquad (4)$$

$$1.9 \times 10^{-3} G_{\mathrm{PCN}} = 5 \times 10^{-2}\, G_{\mathrm{MCSS}} = \, G_{\mathrm{KG}} \qquad (5)$$

Here, subscripts describe the models, N is the segment number, a and σ the segment size, τ the unit time, and G the unit modulus. For KG, the unit of time is the standard time for Lennard-Jones liquids given as $\tau_{\mathrm{KG}} \equiv \sigma_{\mathrm{KG}}\sqrt{m/\epsilon}$. (Here, m is the bead mass, and ϵ is the Lennard-Jones parameter.) For MCSS, the unit time is defined as $\tau_{\mathrm{MCSS}} \equiv \zeta_{\mathrm{MCSS}} b_{\mathrm{MCSS}}^2 / 6k_{\mathrm{B}}T$ with the friction coefficient of the Rouse bead ζ_{MCSS}. (Here, b_{MCSS} is identical to the bond length b in eq 1.) The unit time of PCN is defined with a similar manner with the friction of PCN segment ζ_{PCN}. All the examined models share the unit of energy $k_{\mathrm{B}}T$. Note that eq 5 is incompatible with the unit conversion derived from eq 3 and the energy because of the difference in the stress-optical coefficient[55]. Note also that the presentation of eqs 2-5 is different from the previous publication, though the conversion is the same. (For example, the Kremer-Grest chain with 200 beads corresponds to the MCSS chain with 25 beads and the PCN chain with 5 segments.) Finally, the conversion relationship may change for the MCSS model if the parameters relating to the slip-spring density and its kinetics are different.

RESULTS

In this section, the proposed extended MCSS is evaluated against earlier results reported

for the conventional simulations and experiments. The effects of SHAB shall be discussed in detail in the later section.

Figure 3 shows the diffusion coefficient of 3-arm stars and H polymers as a function of bead numbers per molecule. The earlier result[55] for linear polymers is also shown for comparison. For the H polymers examined, all the subchains for the arms and the backbone have the same bead number. As the diffusion of linear polymers determined the conversion factors given by eqs 2-4, the results reasonably overlap with each other in the top panel. With the same scale-conversion factors, diffusion of star and H branch polymers is also reasonably superposed. As reported by Xu et al. [26], in the small molecular weight regime, diffusion of branch polymers is faster than that for the linear polymer with the same molecular weight because the diffusion has a strong correlation with the gyration radius. Note that for unentangled chains the proposed model exhibits the Rouse-Ham behavior[56,57], in which the diffusion is in inverse proportion of the molecular weight. However, the examined range of molecular weight is in the transitional regime to the entangled behavior. Indeed, even for the small molecular weight regime, the molecular weight dependence of the diffusion constant is stronger than the inverse proportion (shown by dotted line in Fig 3). In the large molecular weight regime, the entanglement

comes into play to suppress the branch polymer diffusion that becomes slower than that for the linear polymer. Such behavior has not been observed for KG even for the simulations with the beads number per molecule of several hundreds, whereas MCSS and PCN reasonably reproduce the phenomenon.

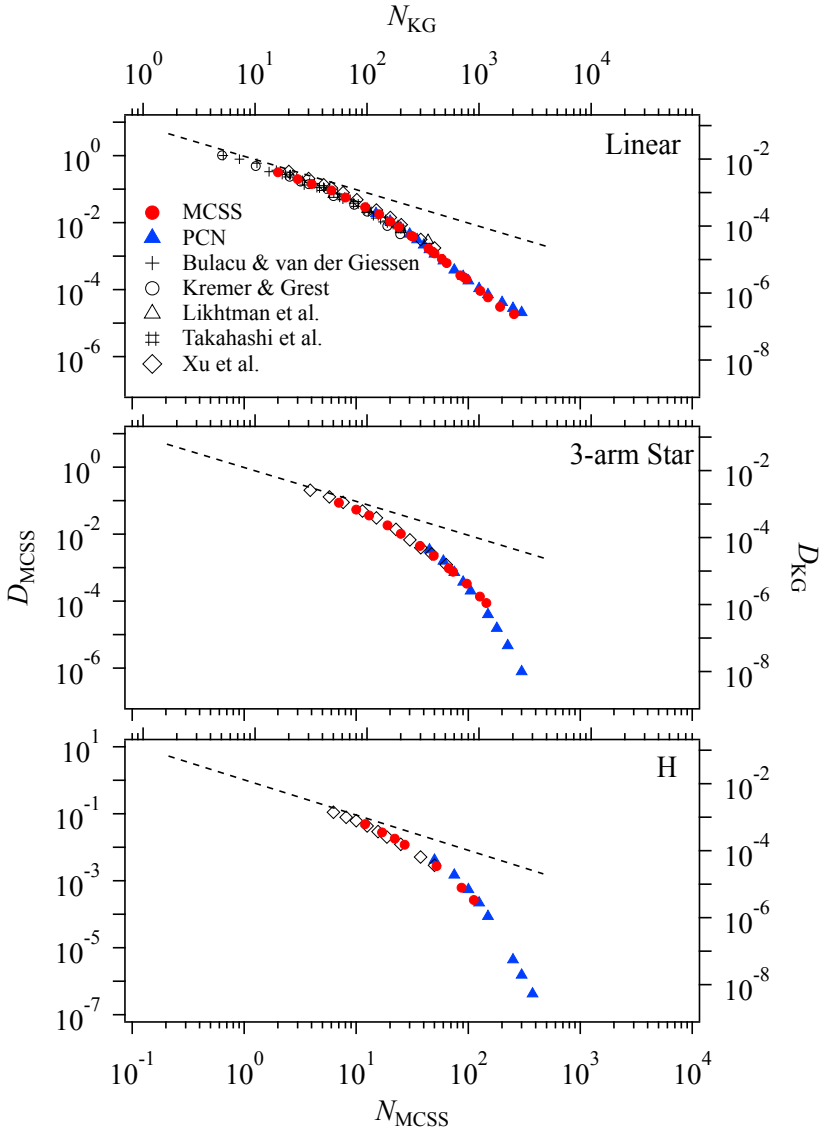

Figure 3 Diffusion coefficient for linear (top), 3-arm star (mid) and H branch (bottom) polymers as a function of total beads number per molecule. The results of MCSS and

PCN simulations are indicated by filled circle and filled triangle, respectively. The other symbols represent the KG results reported earlier[26,31,58–60]. The KG results for star and H polymers are reported by Xu et al[26]. Dotted line shows the slope of -1.

Note that SHAB is essential for H branch polymers. For polymers with multiple branch points, because the backbone chain lies between two branch points, the entanglements formed between backbone chains never relax without SHAB. Indeed, for PCN it has been reported that H polymer melts exhibit solid behaviors when the entanglement network between the backbones percolates throughout the system[15]. For the examined H polymers by MCSS in this study, the backbone network does not percolate because the molecular weight is not sufficiently high. Nevertheless, the simulation results entirely depend on the initial configuration if SHAB is not activated.

It is fair to disclose the inconsistency for the molecular dimension and the scale-conversion factors given by eqs 2 and 3. Figure 4 shows the gyration radius R_g plotted against the segment number per molecule, both in the KG units. As reported for linear polymers[55], due to the lack of excluded volume interactions, R_g in MCSS is smaller than that in KG. Because the discrepancy is not negligible even with the distributions (shown

by error bars), the scale-conversion factors would change if they are determined from the structural measures rather than the diffusion. For such a strategy, detailed tuning of inter-beads interactions and the molecular density in MCSS is necessary, as elaborated recently in comparison to the atomistic models[50,51].

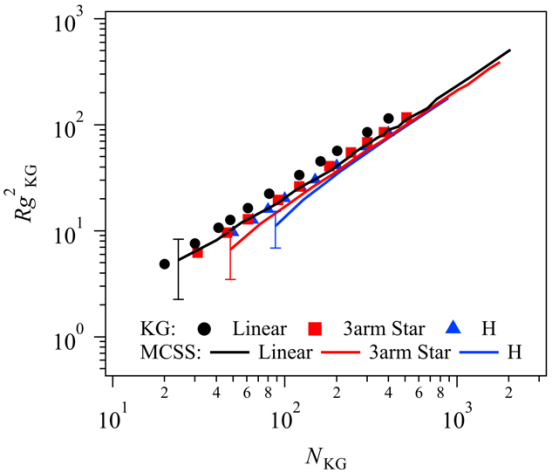

Figure 4 Radius of gyration plotted against the total bead number per molecule for linear (black), 3-arm star (red) and H branch (blue) polymers. The KG and MCSS results are shown by symbols and solid curves. Error bars indicate the distribution for MCSS. The KG results are obtained from Xu et al[26].

Figure 5 shows the zero-shear viscosity of star and H branch polystyrenes as a function of molecular weight. The experimental dataset is extracted from the literature[61,62]. The scale-conversion factors for the polystyrene melts found here are as follows (for the

temperature at 169.5℃).

$$M_{\mathrm{MCSS}} = 1250\ \mathrm{g/mol} \tag{6}$$

$$\tau_{\mathrm{MCSS}}(\mathrm{PS@169.5℃}) = 4 \times 10^{-5}\mathrm{sec} \tag{7}$$

$$G_{\mathrm{MCSS}}(\mathrm{PS@169.5℃}) = 9.1 \times 10^{5}\mathrm{Pa} \tag{8}$$

Note that the M_{MCSS} and $N_{\mathrm{e}}^{\mathrm{SS}} = 3.5$ give the molecular weight between two anchoring points as $M_{\mathrm{e}}^{\mathrm{SS}} = 4375\ \mathrm{g/mol}$. This value is considerably smaller than the typical value of the entanglement molecular weight M_{e} in literature because of the fluctuations imposed around the entanglement. Indeed, the motional constraint realized by the slip-spring is much weaker than the tube and the slip-link, as discussed previously[55]. Nevertheless, as seen in the figures, with the same set of scale-conversion factors, the literature data (shown by cross) are quantitatively reproduced. Similarly to the diffusion, for the small molecular weights, branch polymers exhibit smaller viscosity than the linear polymers with the same molecular weight in relation to the smaller gyration radius[26]. As the molecular weight increases, the viscosity of branch polymers rapidly grows with an exponential manner, and it becomes larger than that for linear polymers in the well-entangled regime. Such behavior is hardly reproduced even by MCSS and barely seen for PCN results.

It is fair to note that the molecular weight range, in which the data for both MCSS and PCN are available and overlapped with each other, is not quite sufficient. The molecular weight range for MCSS is limited due to the computational difficulties. For instance, for the H polystyrene with the molecular weight of 240k (the second leftmost cross in the bottom panel of Fig 5), the computation costs were already impractically large. Further simulations for well-entangled chains are necessary for the evaluation of SHAB.

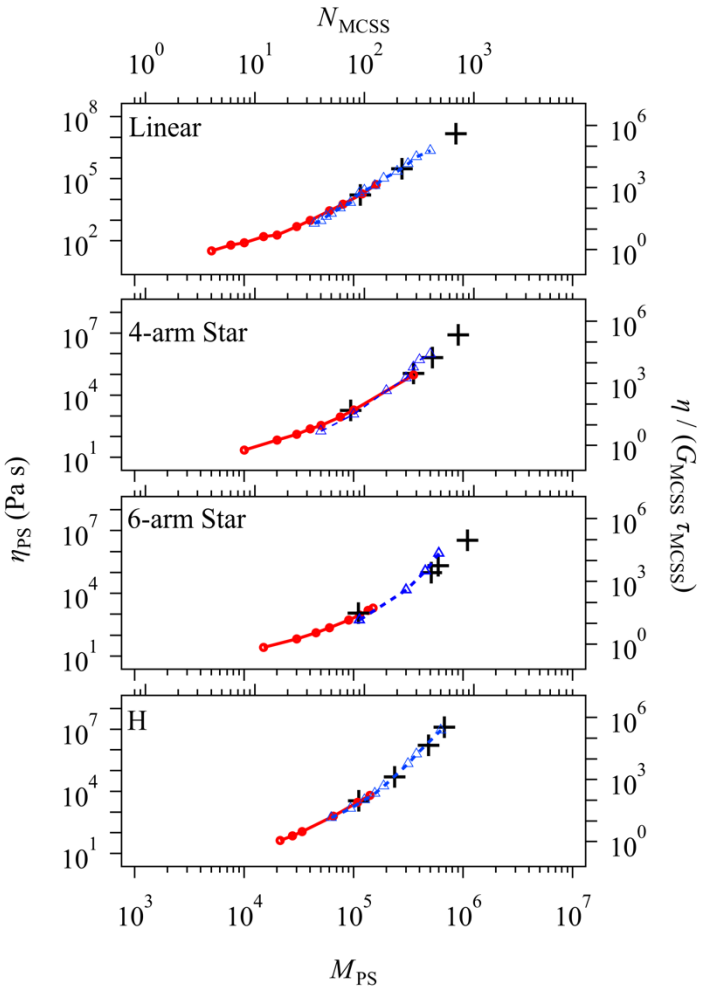

Figure 5 Molecular weight dependence of zero-shear viscosity at 169.5℃ for linear, 4-

arm star, 6-arm star and H branch polystyrene melts from top to bottom. Black cross shows the experimental data extracted from the literature[61,62]. Red circle and blue triangle are the simulation results for MCSS and PCN, respectively.

Figure 6 shows the viscoelasticity of star and H branch polymers obtained from MCSS simulations compared with the literature data for polystyrene melts[61,62]. Although the polydispersity has been reported for the experiment, the simulations were performed for monodisperse systems. Note that for the H polymer examined here, the snapshot is shown in Fig 2. With the scale-conversion parameters in eqs 6-8, the simulation captures the experimental data nicely. (Note that the temperature is identical for Figs 5 and 6.) The simulation results were converted from the stress auto-correlation function by the REPTATE software[63], for which possible uncertainty has been pointed out for the data conversion in the high-frequency domain[64]. Nevertheless, the results are self-consistent.

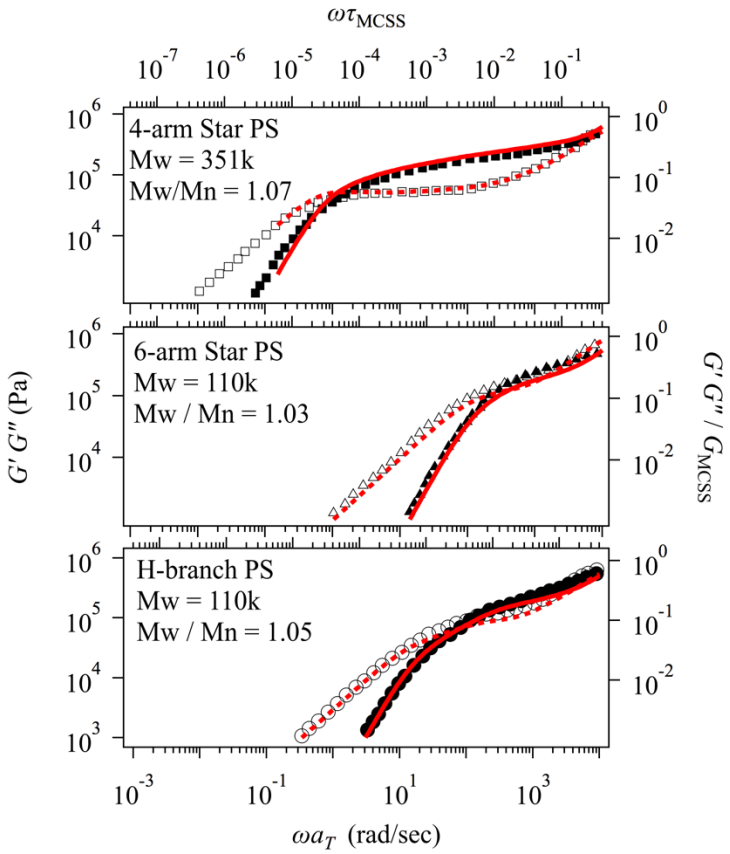

Figure 6 Viscoelasticity of 4-arm (top), 6-arm (mid) and H branch (bottom) polystyrene melts at 169.5℃. The molecular weight and its distribution are indicated in the figure. Filled and unfilled symbols are G' and G'' experimentally reported[61,62]. Solid and broken curves are G' and G'' obtained from the MCSS simulations.

Figure 7 shows the other viscoelastic dataset[65] for linear, symmetric and asymmetric star polystyrene melts, for which the molecular weight of linear polymer is almost twice of the long-arm molecular weight of the star polymers. The polydispersity was not considered in the simulations, although the values experimentally reported are shown in

the figure. Due to some reasons including the difference of temperature, the scale-conversion factors for this case are different from eqs 7 and 8 as follows.

$$\tau_{\mathrm{MCSS}}(\mathrm{PS@130℃}) = 3.3 \times 10^{-2}\mathrm{sec} \quad (9)$$

$$G_{\mathrm{MCSS}}(\mathrm{PS@130℃}) = 1.0 \times 10^{6}\mathrm{Pa} \quad (10)$$

Note that M_{MCSS} is assumed to be constant. It is noteworthy that as reported in the original paper[65], *G*' and *G*" for the asymmetric star polymer is lower than that for the other two polymers in this frequency regime, indicating that the entanglement network is dilated due to the relaxation of the short arm. This behavior is quantitatively captured. However, for the terminal region, the simulation results are discrepant from the experimental data for the star polymers, which exhibit slower relaxation modes. Although the reason is unknown, additional simulations hinted a possible role of molecular weight distribution even though the polydispersity index is small. Further systematic investigations are necessary for this issue, as performed in earlier studies[16,66].

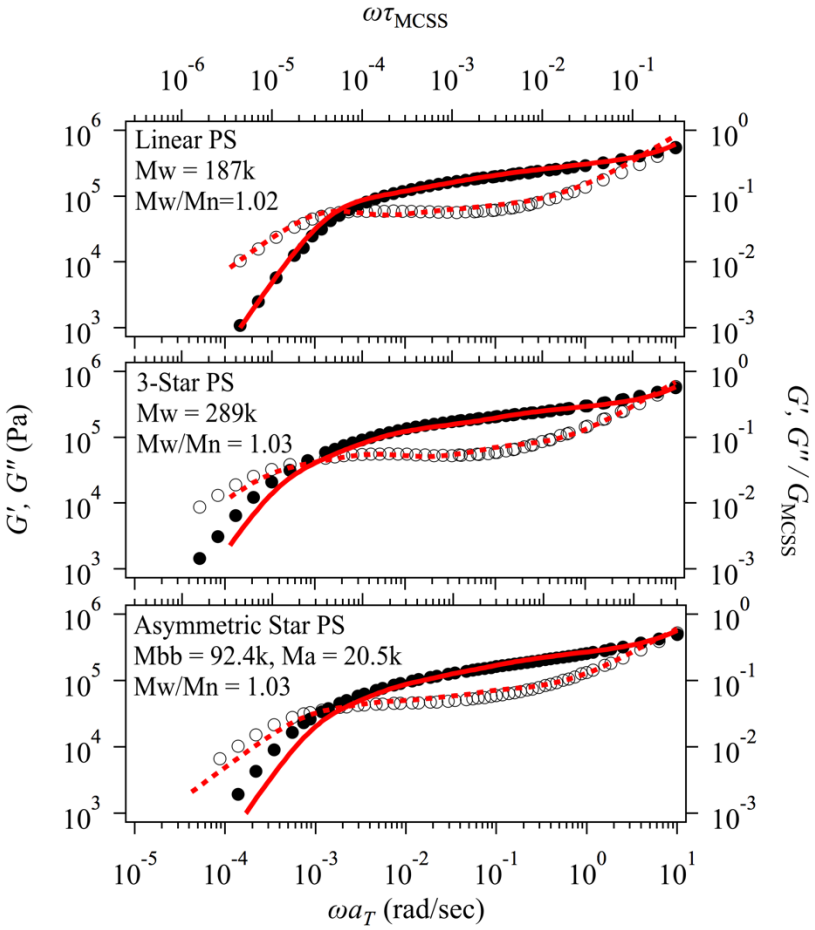

Figure 7 Viscoelasticity of linear (top), 3-arm symmetric star (mid) and 3-arm asymmetric star (bottom) polystyrene melts at 130°C. The molecular weight and its distribution are indicated in the figure. Filled and unfilled symbols are G' and G'' experimentally reported[65]. Solid and broken curves are G' and G'' obtained from the MCSS simulations.

DISCUSSION

For the discussion of the effects of SHAB on the polymer dynamics, the simulations were

performed for a set of asymmetric star polymers, for which the beads number of the two long arms N_{bb} is fixed at 74, whereas that of the short arm N_{a} is varied from 0 to 74. The linear polymer ($N_{\mathrm{a}} = 0$), the symmetric star polymer ($N_{\mathrm{a}} = 74$), and one of the asymmetric star polymers ($N_{\mathrm{a}} = 17$) are the polymers examined in Fig 7.

Figure 8 shows the end-to-end relaxation time for the short and long arms, τ_{a} and τ_{bb}. Apart from these arm relaxation times, the waiting time for SHAB τ_{w} was obtained from the simulations. Namely, for each branch point, the occurrence of SHAB was recorded during the long-time simulation, and τ_{w} was calculated as the averaged interval time between two adjacent SHAB events for each branch point. Although for most of the cases SHAB was triggered by the short arm relaxation, SHAB rarely occurs concerning the long arm relaxation as well. However, such an event was excluded for the calculation of τ_{w}. For the symmetric star with $N_{\mathrm{a}} = 74$, SHAB virtually never occurs and τ_{w} cannot be estimated due to the insufficient statistics. Although all the characteristic times increase with the increasing N_{a}, the N_{a} dependence is different from each other. Namely, τ_{a} exhibits a power-law-like increase with the exponent of ca. 2.5, whereas τ_{w} exhibits exponential growth. These results demonstrate that the Rouse-Ham like relaxation seems dominant for τ_{a} whereas the arm retraction is essential for τ_{w}. The behavior of τ_{a} is

similar to the bead-spring simulation by Zhou and Larson[27], though the examined range of molecular weight is different. Meanwhile, τ_{bb} mildly increases with increasing N_a, reflecting the suppression of the constraint release of the short arm and the occurrence of SHAB along with the increase of N_a.

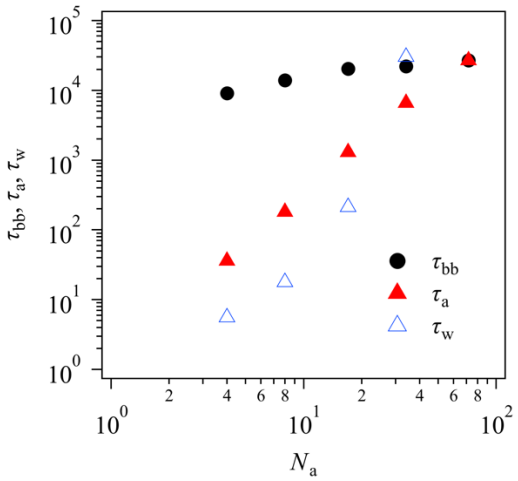

Figure 8 Arm relaxation times plotted against short arm length. Black and red filled symbols indicate the end-to-end relaxation time of backbone and branching arm, respectively. The unfilled symbol is the waiting time for SHAB.

For the efficiency of SHAB, the relation between τ_{bb} and τ_w is essential[40]. For the small N_a chains (with $N_a \leq 17$), SHAB occurs before the long arm relaxation (because $\tau_{bb} > \tau_w$). On the contrary, for the large N_a chains for which $\tau_{bb} < \tau_w$, SHAB never contributes to the long chain relaxation, which is dominated by the arm retraction and the dilation of the network. The PCN simulations have yielded similar results, in which

SHAB affects the dynamics of asymmetric star polymers only when the branching arm is sufficiently shorter than the backbone chains[40].

The effect of SHAB for small N_a polymers can also be discussed in the comparison between the mean-square-displacement of the branch point $g_\mathrm{b}(t)$ and the squared entanglement mesh size[40]. The dilated network mesh size $\xi(t)$ can be related to the survival probability of the slip-links $\varphi(t)$. Let us consider the number of entanglement segment $Z^{\mathrm{SS}} = N/N_\mathrm{e}^{\mathrm{SS}}$, and the entanglement segment length $a_\mathrm{e}^{\mathrm{SS}}$. Because $N_\mathrm{e}^{\mathrm{SS}}$ is the average number of Rouse segments between two anchoring points of slip-springs along the chain, Z^{SS} and $a_\mathrm{e}^{\mathrm{SS}}$ are different from the parameters used in the tube models. Because the chain dimension is not affected by the level of coarse-graining and the inclusion of entanglement, $Z^{\mathrm{SS}}{a_\mathrm{e}^{\mathrm{SS}}}^2 = N a_{\mathrm{MCSS}}^2$. This relation holds for a dilated network, for which the number of entanglement segment and the segment length are given as $Z^{\mathrm{SS}\prime} = N/N_\mathrm{e}^{\mathrm{SS}\prime}$ and $a_\mathrm{e}^{\mathrm{SS}\prime}$. Let us assume that the segment length and the network mesh size are identical to each other, $\xi(t) = a_\mathrm{e}^{\mathrm{SS}\prime}$. Then $Z^{\mathrm{SS}\prime}\xi^2(t) = N a_{\mathrm{MCSS}}^2$. Because $\varphi(t) = Z^{\mathrm{SS}\prime}/Z^{\mathrm{SS}}$, $\xi^2(t)$ can be written with the dilation exponent of unity as[40]

$$\xi^2(t) = \frac{N_\mathrm{e}^{\mathrm{SS}}{a_{\mathrm{MCSS}}}^2}{\varphi(t)} \qquad (10)$$

As mentioned earlier, $N_\mathrm{e}^{\mathrm{SS}}$ for the performed simulations is ca. 3.5. $\varphi(t)$ can be

straightforwardly obtained from the simulations that trace the creation and destruction of all the slip-springs in the system. Figure 9 shows the comparison between $g_{\mathrm{b}}(t)$ and $\xi^2(t)$ for the linear and the star polymers with various N_{a}. For the linear polymer, for which $g_{\mathrm{b}}(t)$ is obtained for the middle bead, $g_{\mathrm{b}}(t)$ is smaller than $\xi^2(t)$ up to a specific time showing that the bead is trapped in the entanglement cage. Because the bead slides out from the cage by the curvilinear diffusion (i.e., reptation motion), $g_{\mathrm{b}}(t)$ becomes larger than $\xi^2(t)$ until the longest relaxation time. Beyond the longest relaxation time, the chain exhibits a free diffusion because $\xi^2(t)$ becomes larger than the chain dimension. For the symmetric star polymer $N_{\mathrm{a}} = 74$, $g_{\mathrm{b}}(t)$ is suppressed in comparison to that for the linear polymer and close to $\xi^2(t)$, demonstrating that the branch point is trapped in the entanglement cage, and the relaxation occurs when $\xi^2(t)$ becomes larger than the molecular dimension. For the asymmetric star polymers, the behavior lies in between those for linear and star polymers depending on the length of the branching arm. Indeed, for the polymers with $N_{\mathrm{a}} \leq 17$, the behavior is similar to that for the linear polymer as indicated by $g_{\mathrm{b}}(t) > \xi^2(t)$. For the polymer with $N_{\mathrm{a}} = 34$, the behavior is mostly the same with that for the symmetric star, for which the branch point diffusion is suppressed. From the results shown in Figs 8 and 9, one may argue that the curvilinear diffusion of the branch point can be analyzed. However, such an analysis

based on the tube framework is complicated for scarcely entangled systems discussed here.

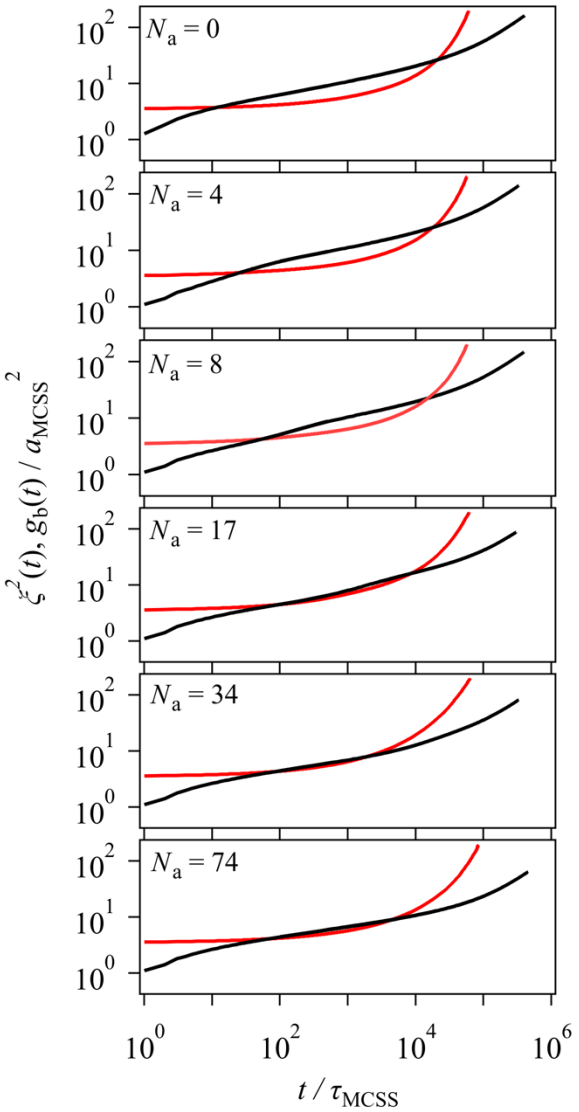

Figure 9 Time development of the squared entanglement mesh size $\xi^2(t)$ (red curve) and the mean-square-displacement of the branch point $g_b(t)$ (black curve) for linear, asymmetric and symmetric star polymers. The bead number of the short arm N_a is indicated in the figure. The bead number of the long arm N_{bb} is fixed at 74.

The effects of SHAB on the polymer dynamics are examined in Figure 10 for the asymmetric star polymers with $N_a = 4$ and 17. For $N_a = 4$ (top panels), $g_b(t)$ and $\xi^2(t)$ are suppressed when SHAB is turned off in the time range of $t > 100\tau_0$. (Interestingly, even without SHAB, $g_b(t)$ is larger than $\xi^2(t)$ due to the mobility of the constraint.) However, SHAB has virtually no effect on the linear relaxation modulus $G(t)$. For N_a =17 (bottom panels), surprisingly, SHAB has no apparent impact on $g_b(t)$, $\xi^2(t)$, and $G(t)$. These results demonstrate that SHAB is effective only for the short branch arms. A similar result was observed for the PCN simulations[40].

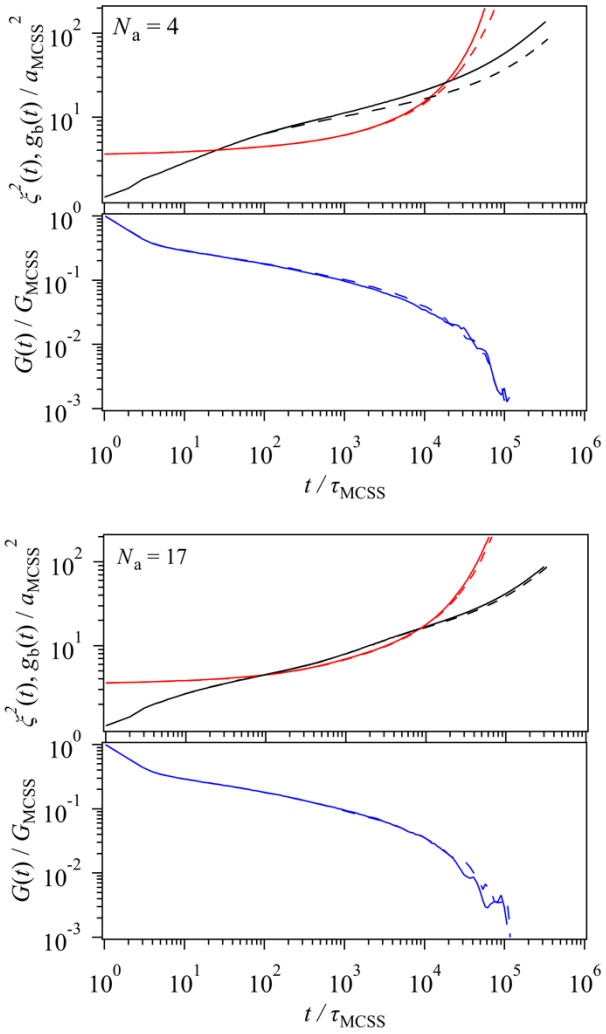

Figure 10 Squared entanglement mesh size $\xi^2(t)$ (red curve), mean-square-displacement of the branch point $g_b(t)$ (black curve), and linear relaxation modulus $G(t)$ (blue curve) for the asymmetric star polymers with the short arm length at $N_a = 4$ (top) and $N_a = 17$ (bottom). The results with and without SHAB are indicated by solid and broken curves, respectively.

Figure 11 shows $g_b(t)$, $\xi^2(t)$, and $G(t)$ for the scarcely entangled H branch polymer

examined in Fig 6. $\xi^2(t)$ shows a two-step relaxation that indicates the relaxations of the arm and the backbone. Without SHAB, since the backbone relaxation never occurs, $\xi^2(t)$ becomes constant after the relaxation of the arms. In spite of this convincing behavior of $\xi^2(t)$, there is no effect of SHAB on $g_{\mathrm{b}}(t)$ and $G(t)$. One of the reasons is that the amount of entanglements formed between the backbones is only 0.04 for this specific case, and the backbone network does not percolate. Although the permanent entanglements create some aggregates like dimers and trimers, for which the relaxation is slower than the single molecule, the effects of such aggregates do not appear in the examined quantities. The reason would be the fact that even with SHAB the aggregates are long-lived, and the relaxation of such aggregates may be similar to those with the permanent links. Note however that the simulation results without SHAB strongly depends on the initial configuration for the formation of entanglements between the backbones. In this specific case, the equilibrated configurations obtained from the simulations with SHAB were employed for both calculations.

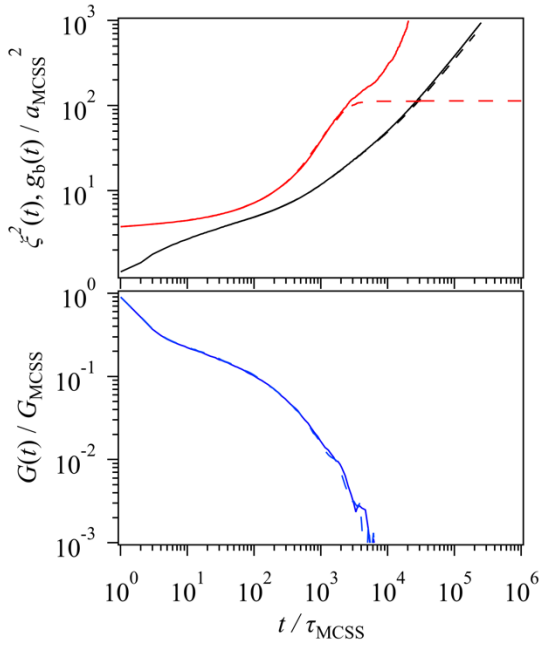

Figure 11 Squared entanglement mesh size $\xi^2(t)$ (red curve), mean-square-displacement of the branch point $g_b(t)$ (black curve), and linear relaxation modulus $G(t)$ (blue curve) for the H polymer examined in Fig 6. The results with and without SHAB are indicated by solid and broken curves, respectively.

The results shown in Figs 10 and 11 reveal that, at least for the examined cases, SHAB has no significant effect on $G(t)$. The results may suggest that the migration of branch point plays a significant role in stress relaxation. However, it should be noted that the results are for scarcely entangled systems, and further examination is necessary for well-entangled systems.

CONCLUSIONS

The multi-chain slip-spring simulation (MCSS) has been extended for branch polymers. In particular, the slip-spring hopping across the branch point (SHAB) has been implemented to activate the relaxation of the backbone after the relaxation of the branching arms. The simulations with the extended MCSS for star and H branch polymers reproduce the experimental data for the diffusion and the linear viscoelasticity. The MCSS results are also consistent with the simulation results performed with the bead-spring model and the primitive chain network model. By the consistency with the experiments and the other simulations, the effects of SHAB were discussed in detail on the diffusion and the relaxation modulus. For the asymmetric star polymers with the significant difference in the molecular weight between the backbone chains and the branching arm, SHAB accelerates the diffusion. For the other star polymers, SHAB has virtually no effect on the diffusion. For the H branch polymer examined in this specific study, although SHAB relaxes the entanglements between the backbone chains, no impact on diffusion has been found. For the viscoelasticity, SHAB does not affect the linear relaxation modulus for the examined polymers. These results may suggest a role of the intrinsic migration of the branch points for scarcely entangled systems. Nevertheless, the results of H branch polymers cannot be obtained without SHAB, which is necessary for the

equilibration of the system.

For the evaluation of SHAB, further tests are necessary. Because the systems used for the test of SHAB are not well-entangled, the criteria for the occurrence of SHAB are fulfilled rather easily. However, for well-entangled systems, further considerations would be necessary for the SHAB criteria, such as the condition of the arm relaxation. Highly asymmetric and well-entangled star polymers and H polymers would be suitable for such evaluations. For such simulations, further improvements of the simulation method for the reduction of computation costs are required, because the level of coarse-graining of MCSS is not that high. In this respect, bead-spring simulations would give useful reference data. The effect of polydispersity is also worth investigating for the evaluation as the constraint-release, and the inter-molecular correlations are naturally considered in the multi-chain model. Studies toward such a direction are ongoing, and the results will be published elsewhere.

Acknowledgment

YM thank Professor Xiaolei Xu, Professor Jizhong Chen, and Professor Lijia An, for kindly providing the dataset for the bead-spring simulation results shown in Figures 3 and

4. YM also thank Professor Qian Huang and Professor Ole Hassager for the experimental data in Figure 7. This study is supported in part by Grant-in-Aid for Scientific Research (A) (17H01152) and for Scientific Research on Innovative Areas (18H04483) from JSPS. The support is also made by the Council for Science, Technology and Innovation, Cross-ministerial Strategic Innovation Promotion Program, "Structural Materials for Innovation" from JST.

REFERENCES

(1) Masubuchi, Y. Simulating the Flow of Entangled Polymers. *Annu. Rev. Chem. Biomol. Eng.* **2014**, *5* (1), 11–33.

(2) de Gennes, P. G. Reptation of a Polymer Chain in the Presence of Fixed Obstacles. *J. Chem. Phys.* **1971**, *55* (2), 572.

(3) Doi, M.; Edwards, S. F. Dynamics of Concentrated Polymer Systems. Part 2. Molecular Motion under Flow. *J. Chem. Soc. Faraday Trans. 2* **1978**, *74*, 1802.

(4) Kuzuu, N.; Doi, M.; Kuzuu, N. Rheology of Star Polymers in Concentrated Solutions and Melts. *J. Polym. Sci. B Polym. Lett. Ed.* **1980**, *18* (12), 775–780.

(5) Pearson, D. S.; Helfand, E. Viscoelastic Properties of Star-Shaped Polymers. *Macromolecules* **1984**, *17* (4), 888–895.

(6) Ball, R. C.; McLeish, T. Dynamic Dilution and the Viscosity of Star-Polymer Melts. *Macromolecules* **1989**, *22* (4), 1911–1913.

(7) Milner, S. T.; McLeish, T. C. B. Parameter-Free Theory for Stress Relaxation in Star Polymer Melts. *Macromolecules* **1997**, *30* (7), 2159–2166.

(8) McLeish, T. C. B. Hierarchical Relaxation in Tube Models of Branched Polymers. *Europhys. Lett.* **1988**, *6* (6), 511–516.

(9) McLeish, T. C. B. Molecular Rheology of H-Polymers. *Macromolecules* **1988**, *21* (4), 1062–1070.

(10) Daniels, D. R.; McLeish, T. C. B.; Crosby, B. J.; Young, R. N.; Fernyhough, C. M. Molecular Rheology of Comb Polymer Melts. 1. Linear Viscoelastic Response. *Macromolecules* **2001**, *34* (20), 7025–7033.

(11) Larson, R. G. Combinatorial Rheology of Branched Polymer Melts. *Macromolecules* **2001**, *34* (13), 4556–4571.

(12) Frischknecht, A. L.; Milner, S. T.; Pryke, A.; Young, R. N.; Hawkins, R.; McLeish, T. C. B. Rheology of Three-Arm Asymmetric Star Polymer Melts. *Macromolecules* **2002**, *35* (12), 4801–4820.

(13) Park, S. J.; Shanbhag, S.; Larson, R. G. A Hierarchical Algorithm for Predicting the Linear Viscoelastic Properties of Polymer Melts with Long-Chain Branching.

Rheol. Acta **2005**, *44* (3), 319–330.

(14) Das, C.; Inkson, N. J.; Read, D. J.; Kelmanson, M. A.; McLeish, T. C. B. Computational Linear Rheology of General Branch-on-Branch Polymers. *J. Rheol. (N. Y. N. Y).* **2006**, *50* (2), 207.

(15) Masubuchi, Y.; Ianniruberto, G.; Greco, F.; Marrucci, G. Primitive Chain Network Simulations for Branched Polymers. *Rheol. Acta* **2006**, *46* (2), 297–303.

(16) van Ruymbeke, E.; Bailly, C.; Keunings, R.; Vlassopoulos, D. A General Methodology to Predict the Linear Rheology of Branched Polymers. *Macromolecules* **2006**, *39* (18), 6248–6259.

(17) Shanbhag, S.; Larson, R. G. A Slip-Link Model of Branch-Point Motion in Entangled Polymers. *Macromolecules* **2004**, *37* (21), 8160–8166.

(18) Bick, D.; McLeish, T. Topological Contributions to Nonlinear Elasticity in Branched Polymers. *Phys. Rev. Lett.* **1996**, *76* (14), 2587–2590.

(19) McLeish, T. C. B.; Larson, R. G. Molecular Constitutive Equations for a Class of Branched Polymers: The Pom-Pom Polymer. *J. Rheol. (N. Y. N. Y).* **1998**, *42* (1), 81.

(20) Karayiannis, N. C.; Mavrantzas, V. G.; Theodorou, D. N. A Novel Monte Carlo Scheme for the Rapid Equilibration of Atomistic Model Polymer Systems of

Precisely Defined Molecular Architecture. *Phys. Rev. Lett.* **2002**, *88* (10), 105503.

(21) Subramanian, G. A Topology Preserving Method for Generating Equilibrated Polymer Melts in Computer Simulations. *J. Chem. Phys.* **2010**, *133* (16), 1–9.

(22) Sliozberg, Y. R.; Andzelm, J. W. Fast Protocol for Equilibration of Entangled and Branched Polymer Chains. *Chem. Phys. Lett.* **2012**, *523*, 139–143.

(23) Grest, G. S.; Fetters, L. J.; Huang, J. S.; Richter, D. Star Polymers: Experiment, Theory, and Simulation. In *ADVANCES IN CHEMICAL PHYSICS*; John Wiley & Sons INC, 1996; pp 67–163.

(24) Brown, S.; Szamel, G. Computer Simulation of Three-Arm Star Polymers. *Macromol. Theory Simulations* **2000**, *9* (1), 14–19.

(25) Di Cecca, A.; Freire, J. J. Simulation of Diffusion and Relaxations of Non-Dilute Star Chains. *Polymer (Guildf).* **2003**, *44* (8), 2589–2597.

(26) Xu, X.; Chen, J.; An, L. Simulation Studies on Architecture Dependence of Unentangled Polymer Melts. *J. Chem. Phys.* **2015**, *142* (7), 074903.

(27) Zhou, Q.; Larson, R. G. Direct Molecular Dynamics Simulation of Branch Point Motion in Asymmetric Star Polymer Melts. *Macromolecules* **2007**, *40* (9), 3443–3449.

(28) Bačová, P.; Moreno, A. J. Real-Space Analysis of Branch Point Motion in Architecturally Complex Polymers. *Macromolecules* **2014**, *47* (19), 6955–6963.

(29) Bačová, P.; Lentzakis, H.; Read, D. J.; Moreno, A. J.; Vlassopoulos, D.; Das, C. Branch-Point Motion in Architecturally Complex Polymers: Estimation of Hopping Parameters from Computer Simulations and Experiments. *Macromolecules* **2014**, *47* (10), 3362–3377.

(30) Jeong, S. H.; Kim, J. M.; Yoon, J.; Tzoumanekas, C.; Kröger, M.; Baig, C. Influence of Molecular Architecture on the Entanglement Network: Topological Analysis of Linear, Long- and Short-Chain Branched Polyethylene Melts via Monte Carlo Simulations. *Soft Matter* **2016**, *12* (16), 3770–3786.

(31) Kremer, K.; Grest, G. S. Dynamics of Entangled Linear Polymer Melts: A Molecular-Dynamics Simulation. *J. Chem. Phys.* **1990**, *92* (8), 5057.

(32) Padding, J. T.; Briels, W. J. Time and Length Scales of Polymer Melts Studied by Coarse-Grained Molecular Dynamics Simulations. *J. Chem. Phys.* **2002**, *117* (2), 925–943.

(33) Kumar, S.; Larson, R. G. Brownian Dynamics Simulations of Flexible Polymers with Spring–Spring Repulsions. *J. Chem. Phys.* **2001**, *114* (15), 6937.

(34) Liu, L.; Padding, J. T.; Den Otter, W. K.; Briels, W. J. Coarse-Grained

Simulations of Moderately Entangled Star Polyethylene Melts. *J. Chem. Phys.* **2013**, *138* (24), 244912.

(35) Zheng, F.; Goujon, F.; Mendonça, A. C. F.; Malfreyt, P.; Tildesley, D. J. Structure and Rheology of Star Polymers in Confined Geometries: A Mesoscopic Simulation Study. *Soft Matter* **2015**, *11* (44), 8590–8598.

(36) Kindt, P.; Briels, W. J. A Single Particle Model to Simulate the Dynamics of Entangled Polymer Melts. *J. Chem. Phys.* **2007**, *127* (13), 134901.

(37) Padding, J. T.; Ruymbeke, E.; Vlassopoulos, D.; Briels, W. J.; van Ruymbeke, E.; Vlassopoulos, D.; Briels, W. J.; Ruymbeke, E.; Vlassopoulos, D.; Briels, W. J. Computer Simulation of the Rheology of Concentrated Star Polymer Suspensions. *Rheol. Acta* **2010**, *49* (5), 473–484.

(38) Masubuchi, Y.; Takimoto, J.-I.; Koyama, K.; Ianniruberto, G.; Marrucci, G.; Greco, F. Brownian Simulations of a Network of Reptating Primitive Chains. *J. Chem. Phys.* **2001**, *115* (9), 4387.

(39) Masubuchi, Y.; Ianniruberto, G.; Greco, F.; Marrucci, G. Molecular Simulations of the Long-Time Behaviour of Entangled Polymeric Liquids by the Primitive Chain Network Model. *Model. Simul. Mater. Sci. Eng.* **2004**, *12* (3), S91–S100.

(40) Masubuchi, Y.; Yaoita, T.; Matsumiya, Y.; Watanabe, H. Primitive Chain

Network Simulations for Asymmetric Star Polymers. *J. Chem. Phys.* **2011**, *134* (19), 194905.

(41) Masubuchi, Y.; Pandey, A.; Amamoto, Y.; Uneyama, T. Orientational Cross Correlations between Entangled Branch Polymers in Primitive Chain Network Simulations. *J. Chem. Phys.* **2017**, *147* (18), 184903.

(42) Masubuchi, Y.; Matsumiya, Y.; Watanabe, H.; Marrucci, G.; Ianniruberto, G. Primitive Chain Network Simulations for Pom-Pom Polymers in Uniaxial Elongational Flows. *Macromolecules* **2014**, *47* (10), 3511–3519.

(43) Masubuchi, Y.; Matsumiya, Y.; Watanabe, H.; Shiromoto, S.; Tsutsubuchi, M.; Togawa, Y. Primitive Chain Network Simulations for Comb-Branched Polymer under Step Shear Deformations. *Rheol. Acta* **2012**, *51* (3), 1–8.

(44) Uneyama, T.; Masubuchi, Y. Multi-Chain Slip-Spring Model for Entangled Polymer Dynamics. *J. Chem. Phys.* **2012**, *137* (15), 154902.

(45) Chappa, V. C.; Morse, D. C.; Zippelius, A.; Müller, M. Translationally Invariant Slip-Spring Model for Entangled Polymer Dynamics. *Phys. Rev. Lett.* **2012**, *109* (14), 148302.

(46) Ramírez-Hernández, A.; Detcheverry, F. A.; Peters, B. L.; Chappa, V. C.; Schweizer, K. S.; Müller, M.; de Pablo, J. J. Dynamical Simulations of Coarse

Grain Polymeric Systems: Rouse and Entangled Dynamics. *Macromolecules* **2013**, *46* (15), 6287–6299.

(47) Langeloth, M.; Masubuchi, Y.; Böhm, M. C.; Müller-plathe, F. Recovering the Reptation Dynamics of Polymer Melts in Dissipative Particle Dynamics Simulations via Slip-Springs. *J. Chem. Phys.* **2013**, *138* (2013), 104907.

(48) Likhtman, A. E. Single-Chain Slip-Link Model of Entangled Polymers: Simultaneous Description of Neutron Spin-Echo, Rheology, and Diffusion. *Macromolecules* **2005**, *38* (14), 6128–6139.

(49) Masubuchi, Y.; Langeloth, M.; Böhm, M. C.; Inoue, T.; Müller-Plathe, F. A Multichain Slip-Spring Dissipative Particle Dynamics Simulation Method for Entangled Polymer Solutions. *Macromolecules* **2016**, *49* (23), 9186–9191.

(50) Vogiatzis, G. G.; Megariotis, G.; Theodorou, D. N. Equation of State Based Slip Spring Model for Entangled Polymer Dynamics. *Macromolecules* **2017**, *50* (7), 3004–3029.

(51) Sgouros, A. P.; Megariotis, G.; Theodorou, D. N. Slip-Spring Model for the Linear and Nonlinear Viscoelastic Properties of Molten Polyethylene Derived from Atomistic Simulations. *Macromolecules* **2017**, *50* (11), 4524–4541.

(52) Schieber, J. D. Fluctuations in Entanglements of Polymer Liquids. *J. Chem.*

Phys. **2003**, *118* (11), 5162.

(53) Hua, C. C.; Schieber, J. Segment Connectivity, Chain-Length Breathing, Segmental Stretch, and Constraint Release in Reptation Models. I. Theory and Single-Step Strain Predictions. *J. Chem. Phys.* **1998**, *109* (22), 10018–10027.

(54) Ramírez-Hernández, A.; Peters, B. L.; Schneider, L.; Andreev, M.; Schieber, J. D.; Müller, M.; Kröger, M.; De Pablo, J. J. A Detailed Examination of the Topological Constraints of Lamellae-Forming Block Copolymers. *Macromolecules* **2018**, *51* (5), 2110–2124.

(55) Masubuchi, Y.; Uneyama, T. Comparison among Multi-Chain Models for Entangled Polymer Dynamics. *Soft Matter* **2018**, *14* (29), 5986–5994.

(56) Rouse, P. E. A Theory of the Linear Viscoelastic Properties of Dilute Solutions of Coiling Polymers. *J. Chem. Phys.* **1953**, *21* (7), 1272.

(57) Ham, J. S. Viscoelastic Theory of Branched and Cross-Linked Polymers. *J. Chem. Phys.* **1957**, *26* (3), 625–633.

(58) Bulacu, M.; van der Giessen, E. Effect of Bending and Torsion Rigidity on Self-Diffusion in Polymer Melts: A Molecular-Dynamics Study. *J. Chem. Phys.* **2005**, *123* (11), 114901.

(59) Likhtman, A. E.; Sukumaran, S. K.; Ramirez, J. Linear Viscoelasticity from

Molecular Dynamics Simulation of Entangled Polymers. *Macromolecules* **2007**, *40* (18), 6748–6757.

(60) Takahashi, K. Z.; Yamato, N.; Yasuoka, K.; Masubuchi, Y. Critical Test of Bead–Spring Model to Resolve the Scaling Laws of Polymer Melts: A Molecular Dynamics Study. *Mol. Simul.* **2017**, *43* (13–16), 1196–1201.

(61) Graessley, W. W.; Roovers, J. Melt Rheology of Four-Arm and Six-Arm Star Polystyrenes. *Macromolecules* **1979**, *12* (5), 959–965.

(62) Roovers, J. Melt Rheology of H-Shaped Polystyrenes. *Macromolecules* **1984**, *17* (6), 1196–1200.

(63) Likhtman, A.; Ramirez, J. REPTATE.

(64) Tassieri, M.; Ramírez, J.; Karayiannis, N. C.; Sukumaran, S. K.; Masubuchi, Y. I-Rheo GT : Transforming from Time to Frequency Domain without Artifacts. *Macromolecules* **2018**, *51* (14), 5055–5068.

(65) Huang, Q.; Agostini, S.; Hengeller, L.; Shivokhin, M.; Alvarez, N. J.; Hutchings, L. R.; Hassager, O. Dynamics of Star Polymers in Fast Extensional Flow and Stress Relaxation. *Macromolecules* **2016**, *49* (17), 6694–6699.

(66) Kapnistos, M.; Vlassopoulos, D.; Roovers, J.; Leal, L. G. Linear Rheology of Architecturally Complex Macromolecules: Comb Polymers with Linear

Backbones. *Macromolecules* **2005**, *38* (18), 7852–7862.

(67) Lee, J. H.; Fetters, L. J.; Archer, L. A. Branch-Point Motion in Asymmetric Star Polymers. *Macromolecules* **2005**, *38* (10), 4484–4494.

(68) Chen, X.; Larson, R. G.; Xue, C.; Larson, R. G.; Chen, X.; Larson, R. G. Effect of Branch Point Position on the Linear Rheology of Asymmetric Star Polymers. *Macromolecules* **2008**, *41* (19), 6871–6872.

(69) McLeish, T. C. B.; Allgaier, J.; Bick, D. K.; Bishko, G.; Biswas, P.; Blackwell, R.; Blottiere, B.; Clarke, N.; Gibbs, B.; Groves, D. J.; et al. Dynamics of Entangled H-Polymers: Theory, Rheology, and Neutron-Scattering. *Macromolecules* **1999**, *32* (20), 6734–6758.

for Table of Contents use only